Hindawi
Laser and Particle Beams
Volume 2021, Article ID 8815697, 7 pages
https://doi.org/10.1155/2021/8815697

CAMBRIDGE
UNIVERSITY PRESS

Research Article

Determination of the Pulsed Electron Beam Spectrum by Current and Voltage Oscillograms

A. Pushkarev,[1] **A. Prima**,[1] **V. Ezhov**,[1] **I. Miloichikova**,[1,2] **and E. Petrenko**[1]

[1]*Tomsk Polytechnic University, 634050 Tomsk, Russia*
[2]*Cancer Research Institute of Tomsk NRMC RAS, Kooperativny Street 5, 634050 Tomsk, Russia*

Correspondence should be addressed to A. Pushkarev; aipush@mail.ru

Received 29 September 2020; Revised 28 November 2020; Accepted 19 December 2020; Published 9 January 2021

Academic Editor: T. Shao

The algorithm and results of calculating the integral and differential energy spectra of a pulsed electron beam (350–500 keV, 80 ns), generated by direct-action accelerators, are presented. The electron spectrum was calculated using the oscillograms of the accelerating voltage, electron current, total current of the diode, and the one-dimensional Child–Langmuir (1D CL) ratio. It was found that the discrepancy in the integrated electron beam energy spectrum, when measured using the total current in the diode and using the electron beam current, did not exceed 15% for 80%–95% of the electrons generated in a diode with graphite, carbon fabric, and multipoint cathodes. When calculating the electron spectrum using the 1D CL, the error was much higher.

1. Introduction

For technological applications, pulsed electron beams with high current density (more than 100 A/cm^2) and high energy density, which generate direct-action accelerators (with vacuum electron diode) with an explosive-emission cathode, are widely used [1, 2]. The beam energy spectrum of electrons or ions is an important parameter of the charged particle beam generator. The energy spectrum of electrons and ions determines the penetration depth into a target and the absorbed dose distribution [3, 4]. When pulsed electron beams are used to initiate plasma chemical processes, the electron spectrum influences the kinetics and selectivity of chemical reactions [5]. The composition and energy spectrum of the ions in the beam significantly influence the distribution profile by the depth when doping [6] and for radiation defects generation in the target at simulated radiation irradiation [7, 8], etc. Therefore, the operational control of the energy spectrum of charged particles is an important factor in the beam-plasma technologies and installations for their implementation.

Special sensors are mainly used to measure the energy spectrum of charged particle beams. In [9], a method of determining the electron beam energy spectrum from Cherenkov radiation generated in the microwave range is presented. In [10], thermal imaging diagnostics of pulsed electron beams is presented. It provides an energy density distribution measurement of the electron beam along the cross section, electron energy spectrum measurement, etc. To measure the energy spectrum of electrons, the distribution of the absorbed dose over the depth of a target (made of a material with a low density and low thermal conductivity) is analysed. To measure the electron beam energy spectrum, a magnetic spectrometer was designed [11]. To record the electron's distribution after moving half a circle driven by Lorentz force, an imaging plate was placed perpendicular to the incident direction of the electron beam by the side of a 1 mm diameter collimator hole. The energy spectrum of the pulsed electron beam generated by the direct-action accelerator is calculated from the accelerating voltage and electron current oscillograms [12]. At an electron energy of more than 10 keV (speed exceeds 6 cm/ns), the delay between the oscillograms of accelerating voltage and the electron current is insignificant, even at a distance of 5–10 cm from the diode to the electron current sensor—Faraday cup (FC). However, these methods do not provide an operational measurement of the electron beam parameters without stopping the technological process (nondestructive

diagnostics). The application of the Rogowski coil (RC) for electron current measurement is limited by the use of a leading magnetic field for the electron beam or by the reverse current through the plasma channel when the beam is output to the gas [13].

For the operational and nondestructive control of the electron beam spectrum, it is possible to use the total diode current. The performed current balance analysis in the accelerator diode assembly showed that when generating the electron beam, the total current was more than the electron beam current. The losses are mainly due to electron scattering in the A-K gap. In the mode of matching the diode impedance with the output resistance of the pulse generator, the current loss did not exceed 12% [14, 15].

For the operational and nondestructive control of the electron beam spectrum, it is possible to use also the one-dimensional Child–Langmuir (1D CL) ratio [16]. Studies of the vacuum diode in generating a high-current electron beam have shown that the electron current is limited by the emission capacity of the cathode or the space charge of electrons in the A-K gap [1, 17]. When forming cathode plasma with high concentration, the electron current density is described by 1D CL. The results of the experimental study of a flat diode with explosion-emission graphite, copper, and carbon fabric cathodes and a multipoint W cathode are presented in [18]. The tests were performed on a TEU-500 accelerator (350–500 kV, 80 ns) [14]. In addition, studies of a strip diode with a graphite cathode, in the mode of electron self-magnetic insulation, were performed on a TEMP-4M accelerator (150–200 kV, 400–600 ns) [19]. In the tested diodes, a satisfactory coincidence of the experimental values of the total current with those calculated from 1D CL (for the working area of the cathode) was observed, not only in the absence of a change in the electron trajectory in the A-K gap but also in its deviation from the normal to the cathode surface by an angle of less than 90° (without magnetic electron cutoff). The increase in electron current due to the reduction of the A-K gap, the increase in cathode emission area by cathode plasma, and the presence of microcavities on the cathode are well described by 1D CL, taking into account the increase of cathode emission surface area and reduction of the A-K gap. In [11], a method of the energy spectrum of pulsed electron beam calculation from the accelerating voltage (using Child–Langmuir law) is presented. However, this method is only applicable to diodes operating in the mode of limiting the current by a space charge in the A-K gap. In addition, this method does not allow the summation of the electrons with the same energy, which are generated during the front and rear edges of the pulse.

The purpose of the performed studies is to develop a nondestructive method by studying the energy spectrum of the pulsed electron beam generated by direct-action accelerators, which allow the summation of the electrons with the same energy, which are generated during the front and rear edges of the pulse.

2. Experimental Setup and Methods

Investigations of the electron beam energy spectrum were performed on a TEU-500 pulse accelerator (350–500 kV, 80 ns) [14]. Figure 1 shows the accelerator diode assembly and location of the diagnostic equipment.

We used a diode with a 45 mm diameter flat cylindrical cathode made of different materials. As the anode, we used a 92 mm diameter flat copper FC collector. To measure the total current in the diode, a Rogowski coil with reverse turn was used. The acceleration voltage was measured by a capacitive divider located in the oil-filled chamber and a differential voltage divider located in the vacuum volume of the diode chamber [20]. The total electron beam current was measured by a Faraday cup, which was pumped along with the diode chamber at a pressure of 0.05–0.1 Pa. The FC collector with a diameter of 92 mm was connected to the FC chamber by a low-inductive shunt with a resistance of 0.05 Ohms. Calibration showed that the diagnostic equipment of the diode assembly correctly reflected its operation in the short circuit mode, when operating on a resistive load of up to 60 Ohms, and when operating on a diode.

3. Electron Spectrum Determination

3.1. Determination of Electron Beam Spectrum using the Current Oscillograms. Figure 2 shows the characteristic oscillograms of the accelerating voltage, the total current of the diode assembly, and the electron beam current.

When calculating the integrated electron beam energy spectrum, at first in the program OriginPro 9.0 [21], a spreadsheet of the dependence of electron current on accelerating voltage was built. Then, in the spreadsheet, the values of accelerating voltage and current were sorted synchronously in the order of voltage increase ("sort columns/ascending"). Next, the electron current was integrated over time, which allowed the summation of the electrons with the same energy which are generated during the front and rear edges of the pulse. The charge of the electrons was then recalculated on their number, and the integral dependence of the number of electrons on their energy (which is equal to the product of the electron charge on the accelerating voltage) was built. Figure 3 shows the calculation results.

With a total electron beam charge per pulse of 0.5–0.8 mC, the total number of electrons in the beam was $(3–5) \cdot 10^{15}$. At the same time, 80% of the electrons had an energy of more than 200 keV.

The approximation of the integrated electron beam energy spectrum by the polynomial and subsequent differentiation enables the distribution of electrons by the energy in the beam (electron beam energy spectrum) to be obtained, as shown in Figure 4.

The electron beam energy spectrum calculated using the electron current was further used to evaluate the correctness

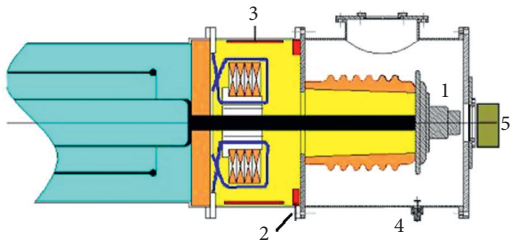

FIGURE 1: Diode assembly diagram and location of the diagnostic equipment: (1) cathode; (2) Rogowski coil; (3) capacitive voltage divider; (4) differential divider; (5) Faraday cup.

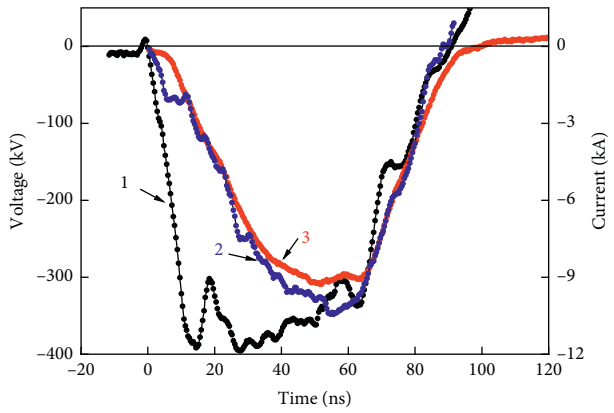

FIGURE 2: Oscillograms of the accelerating voltage (1), diode assembly total current (2), and electron beam current (3) (using graphite cathode).

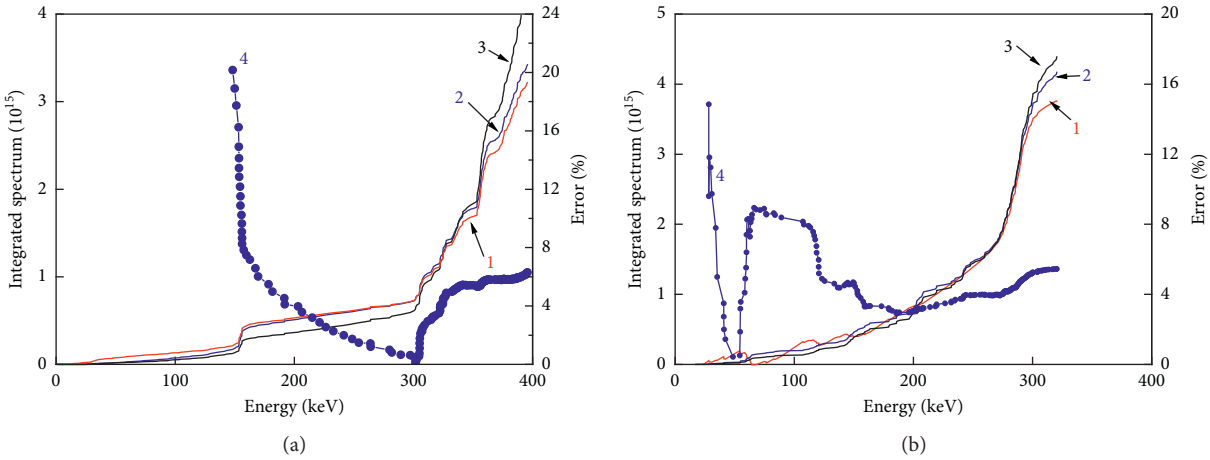

FIGURE 3: The integrated electron beam spectrum calculated using the electron current (1), using the total current in the diode assembly (2), and using the 1D CL (3). The error in calculating the electron beam spectrum using the total current (4). Graphite cathode (a) and carbon fabric cathode (b).

of electron spectrum measurements by other methods—using the total current of the diode or one-dimensional Child–Langmuir ratio.

Figures 3 and 4 show also the electron beam energy spectrum calculated using the total current of the diode unit. The calculation was made according to the algorithm, which was used to calculate the electron beam spectrum using the electron current oscillograms. Figure 3 shows the error in calculating the integrated electron beam spectrum. Error was calculated from the following equation:

$$Er_1(E) = \frac{100\left|N_{RC}(E) - N_{FC}(E)\right|}{N_{FC}(E)},\ \%, \qquad (1)$$

where $N_{RC}(E)$ is the number of electrons with energy from 0 to E, calculated from the total current of the diode, and N_{FC}

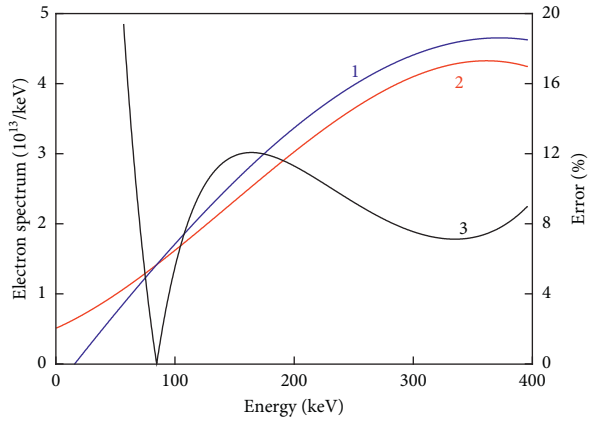

FIGURE 4: An electron beam energy spectrum calculated using the total current in the diode assembly (1) and using the electron current (2). The error of calculation of electron beam spectrum (3) (using graphite cathode).

(E) is the number of electrons with energy from 0 to E, calculated from the electron current.

Figure 4 shows the error in calculating the electron beam energy spectrum. Error was calculated from the following equation:

$$Er_2(E) = \frac{100\left|n_{RC}(E) - n_{FC}(E)\right|}{n_{FC}(E)},\ \%, \qquad (2)$$

where n_{RC} (E) is the number of electrons with energy E, calculated from the total current of the diode, and n_{FC} (E) is the number of electrons with energy E, calculated from the electron current.

The developed algorithm allows us to determine the change in the spectrum of electrons in the beam when exiting the diode chamber. Figure 5 shows the integrated electron beam spectrum of the original electron beam and the extracted beam.

In this series of experiments, a stainless-steel lattice with a transparency of 70% was used as the anode. The FC collector was 5 mm behind the lattice. Studies show that the anode array only weakens the electron beam without changing its energy spectrum. After passing the 0.13 mm thick aluminium foil, the beam spectrum varies significantly in the low energy region.

3.2. Determination of Electron Beam Energy Spectrum Using the 1D CL. Studies have shown that when operating a vacuum electron diode in the space-charge-limited current mode, the calculation of the electron beam spectrum by CL 1D also produces correct results (see Figure 3). The calculation of the integrated electron beam energy spectrum is made according to the algorithm of spectrum calculation in Figure 3, but instead of the electron current, the calculated current by 1D CL is used. Considering that the A-K gap reduction and cathode area increase at emission surface expansion, the electron current is equal to [18]

$$I_{CL}(t) = \frac{2.33 \cdot 10^{-6} \pi F \cdot U(t)^{3/2} \left(r_0 + vt\right)^2}{\left(d_0 - vt\right)^2}, \qquad (3)$$

where U is the accelerating voltage, d_0 is the initial A-K gap, r_0 is the initial radius of the cathode, v is the cathode plasma expansion velocity, and F is the form factor.

In contrast to a smooth emitting surface for which the 1D CL formula was obtained, the cathode surface may have microirregularities. If the cathode-surface roughness exceeds the thickness of the space charge layer, the emission area of the cathode increases and it is necessary to introduce a form factor $F > 1$ [18].

The performed studies showed that the difference in the integrated electron beam energy spectrum, when measured using the total current in the diode and using the electron beam current, does not exceed 15% for 80–95% of the beam electrons and for 95% of the beam energy. The error of electron beam spectrum calculation using the total current in the diode is most significant in the field of low electron energies. The electron beam spectrum calculation by 1D CL also allows for correct results, but the error is higher.

3.3. Thermal Imaging Diagnostics of an Electron Beam Spectrum. The distribution of the absorbed dose over the depth of the target depends on the energy spectrum of electrons in the beam, so thermal imaging diagnostics can be used to measure the energy spectrum of the electrons [10]. To measure the distribution of the absorbed electron beam dose by depth, in a cylindrical target from foamed polystyrene, a section by diameter was made. After irradiation of the target with a pulsed electron beam, the cut target was opened and a thermal image of its inner surface was recorded, 2-3 seconds after irradiation. Due to the low thermal conductivity of the target material, its temperature distribution change was no more than 5% during the first 3 seconds [10]. In this series of experiments, the distribution of the absorbed dose over the depth of the target was measured for a beam extracted from the diode chamber into the atmosphere through an aluminum foil.

Figure 6 shows the oscillograms of accelerating voltage generated by the TEU-500 accelerator in this series of experiments and the thermograms of an internal surface of the

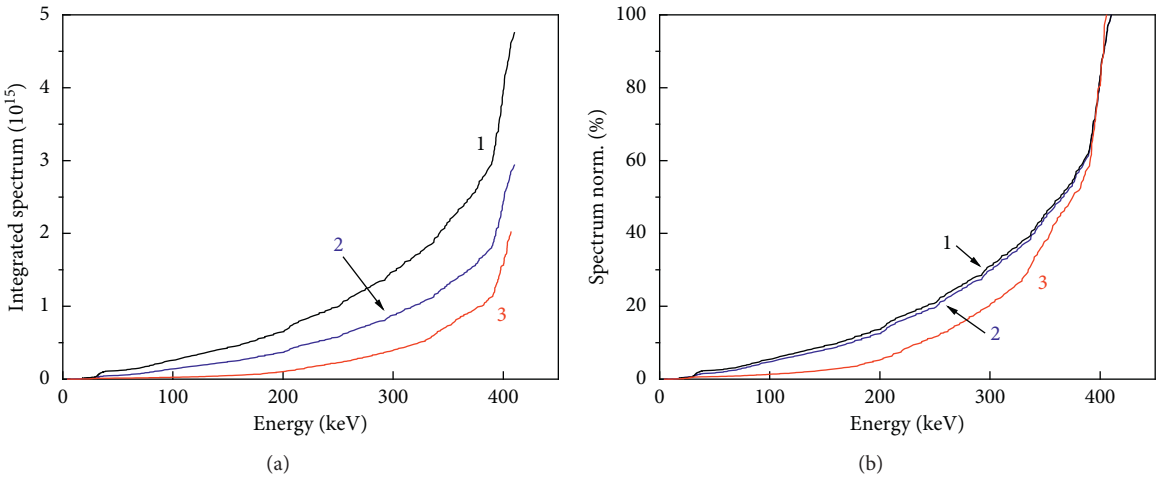

FIGURE 5: Integrated electron beam spectrum calculated using the total current in the diode unit (1), using the electron current measured behind anode (2), and using the electron current measured behind anode and aluminium foil (3). Absolute (a) and normalised (b) values (using carbon fabric cathode).

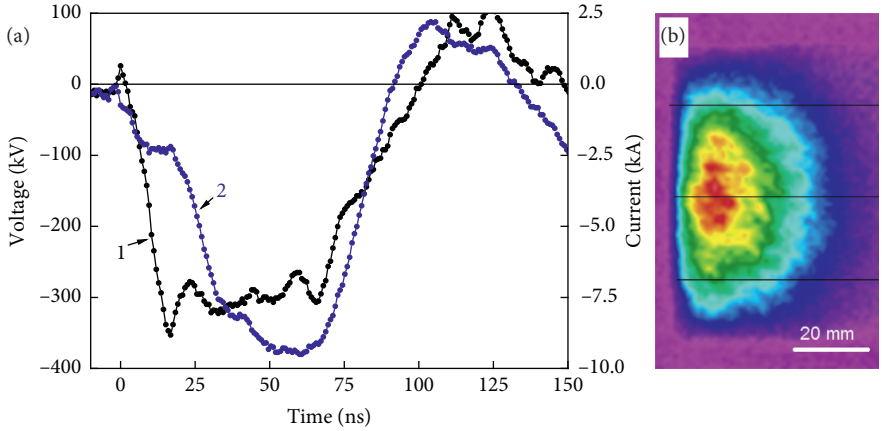

FIGURE 6: Oscillograms of accelerating voltage (1) and full current (2) in the diode (a) and thermogram of a target (b) (using graphite cathode).

target (one pulse). The diameter of the target is 85 mm, the thickness is 110 mm, and the direction of electron movement goes left to right (see Figure 1).

The thermogram was processed according to the program SmartView 4.1 Fluke Corporation [22], and the absorbed dose of the electron beam was calculated from heating of the target:

$$D(x, y) = c_v \Delta T(x, y), Gr, \quad (4)$$

where c_v is the target specific heat and ΔT is the target heating.

Figure 7 shows the normalised absorbed dose distribution over the depth of the target for three cross sections (see Figure 6) and the results of the simulation of the absorption of a monoenergetic electron beam in foamed polystyrene with a density of 0.018 g/cm^3, according to Geant4 program [23]. The simulation is made for an electron beam with a diameter of 5 cm and with a constant electron fluency across the cross section.

Figure 8 shows the results of the integrated electron beam spectrum calculation for Figure 6(a).

Studies have shown that the distribution of the electron beam absorbed dose generated by the TEU-500 accelerator over the depth of the foamed polystyrene target corresponds to the electron beam energy spectrum.

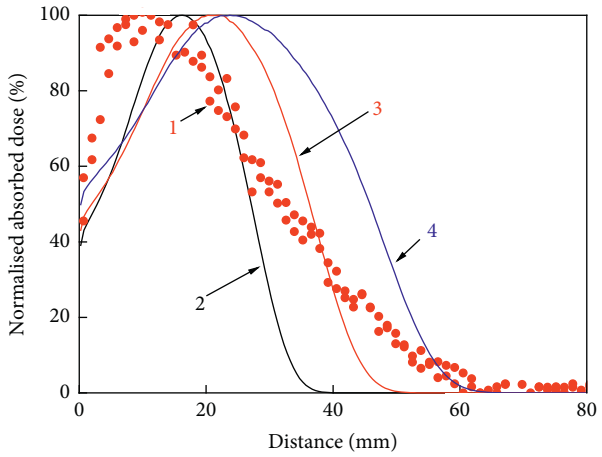

FIGURE 7: Normalised absorbed dose distribution over the depth of the target for three cross sections in Figure 6(b) (1, points). Results of simulation absorption dose distribution of electrons with energy 250 keV (2), 300 keV (3), and 350 keV (4).

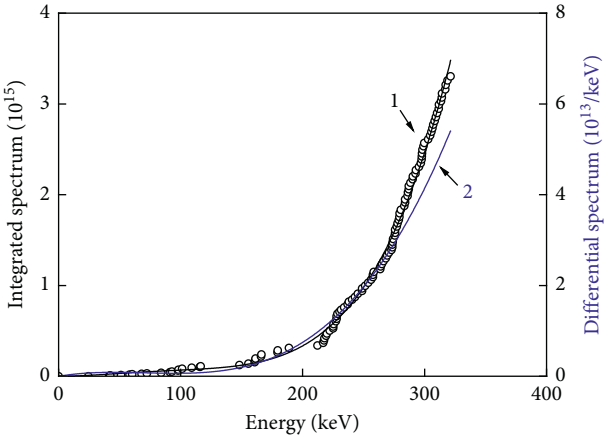

FIGURE 8: Integrated electron beam spectrum (1) and electron beam spectrum (2) calculated using the 1D CL.

4. Conclusion

The developed technique for diagnosing the distribution of charged particles by the energy in the beam (beam energy spectrum), which generates a direct-action accelerator, enables the control of the parameters quickly and accurately during the technological process. Spectrum control does not require additional sophisticated equipment and lengthy processing of measurement results. The technique has been successfully tested on various accelerators that form pulsed electron beams.

The discrepancy in the integrated electron beam energy spectrum when measured using the total current in the diode and using the electron beam current does not exceed 15% for 80–95% of the electrons generated in the diode with graphite, carbon fabric, and multipoint cathodes. When calculating the electron spectrum using the 1D CL, the error is much higher.

The developed technique does not include the energy spread of the beam, due to space charge, scattering, or other effects.

Data Availability

The data used to support the findings of this study are available on request from the corresponding author.

Conflicts of Interest

The authors declare that they have no conflicts of interest.

Authors' Contributions

All authors contributed equally to this work.

Acknowledgments

This study was supported by the Russian Foundation for Basic Research, project nos. 19-38-90001 and 19-38-90071.

References

[1] S. P. Bugaev, Y. I. Krenydel, and P. M. Shanin, *Electron Beams of a Wide Profile*, M Energoatomizdat, in Russian, 1984.

[2] G. A. Mesyats, *Pulsed Power Engineering and Electronics,* M., p. 704, Nauka, 2004.

[3] S. Humphries, *Charged Particle Beams*, Wiley, New York, NY, USA, 1990.

[4] P. Sigmund, "Particle penetration and radiation effects. general aspects and stopping of swift point charges," in *Springer Series Solid-State Science*sp. 437, Springer, Berlin, Germany, 2005.

[5] V. D. Rusanov and A. A. Fridman, *Physics of Chemically Active Plasma*, CRC Pr I Llc, Boca Raton, FL, USA, 2007.

[6] J. M. Poate, G. Foti, and D. C. Jacobson, *Surface Modification and Alloying by Laser, Ion, and Electron Beams*, Springer, Berlin, Germany, 2013.

[7] G. S. Was, *Fundamentals of Radiation Materials Science. Metals and Alloys*, Springer, Berlin, Germany, 2017.

[8] S. J. Zinkle and L. L. Snead, "Opportunities and limitations for ion beams in radiation effects studies: bridging critical gaps between charged particle and neutron irradiations," *Scripta Materialia*, vol. 143, pp. 154–160, 2018.

[9] K. A. Trukhanov, V. V. Poliektov, and V. I. Shvedunov, "Theoretical and experimental study of beam energy spread diagnostics with Vavilov–Cherenkov radiation at optical and RF wavelength," in *Proceedings XIX Russian Particle Accelerator Conference RuPAC'2004*, pp. 106–108, Geneva, Switzerland, October 2004.

[10] A. Pushkarev, G. Kholodnaya, R. Sazonov, and D. Ponomarev, "Thermal imaging diagnostics of high-current electron beams," *Review of Scientific Instruments*, vol. 83, no. 10, p. 103301, 2012.

[11] J. Shen, H. H. An, H. Y. Liu et al., "Energy spectrum analysis for intense pulsed electron beam," *Laser and Particle Beams*, vol. 34, no. 4, pp. 742–747, 2016.

[12] P. Bystrov, A. Prokopenko, Y. Pavlov, and N. Rozanov, "Computer program "BEAM SCANNING" for calculation of irradiation processes in radiation-technological installations," *Procedia Computer Science*, vol. 145, pp. 123–133, 2018.

[13] G. E. Ozur, "On the current of the low-energy high-current electron beam formed in a plasma-filled diode," *IEEE Transactions on Plasma Science*, vol. 37, no. 10, pp. 1897–1900, 2009.

[14] A. I. Pushkarev, Y. N. Novoselov, and R. V. Sazonov, "Losses in a pulsed electron beam during its formation and extraction from the diode chamber of an accelerator," *Instruments and Experimental Techniques*, vol. 50, no. 5, pp. 687–694, 2007.

[15] A. I. Pushkarev, A. I. Prima, Yu.I. Egorova, and V. V. Ezhov, "Diagnostics of pulsed beams of electrons, ions, and atoms," *Instruments and Experimental Techniques*, vol. 3, pp. 5–24, 2020.

[16] I. Langmuir, "The effect of space charge and residual gases on thermionic currents in high vacuum," *Phys. Rev.*, vol. 2, pp. 45–51, 1913.

[17] G. A. Mesyats and D. I. Proskurovsky, *Pulsed Electrical Discharge in Vacuum*, Springer-Veriag, New York, NY, USA, 1989.

[18] A. I. Pushkarev, Y. I. Isakova, and I. P. Khailov, "The influence of a change in the electron trajectory in the vacuum-diode anode-cathode gap on the impedance," *Instruments and Experimental Techniques*, vol. 59, no. 4, pp. 544–550, 2016.

[19] A. I. Pushkarev and Y. I. Isakova, "A gigawatt power pulsed ion beam generator for industrial applications," *Surface and Coatings Technology*, vol. 228, pp. S382–S384, 2013.

[20] Y. I. Isakova, A. I. Pushkarev, and G. E. Kholodnaya, "A differential high-voltage divider," *Instruments and Experimental Techniques*, vol. 54, no. 2, pp. 183–186, 2011.

[21] OriginPro 9.0: https://www.originlab.com.

[22] Fluke Corporation: https://www.fluke.com.

[23] Collaboration GEANT, *Physics Reference Manual, Version: GEANT4*, vol. 9, p. 563, 2005.